JOURNAL OF VIROLOGY, July 2001, p. 6625–6634 Vol. 75, No. 14
0022-538X/01/$04.00+0 DOI: 10.1128/JVI.75.14.6625–6634.2001

A Monoclonal Antibody Specific for Reovirus Outer-Capsid Protein σ3 Inhibits σ1-Mediated Hemagglutination by Steric Hindrance

EMMA L. NASON,[1] J. DENISE WETZEL,[2,3] S. K. MUKHERJEE,[1] ERIK S. BARTON,[3,4] B. V. VENKATARAM PRASAD,[1]* AND TERENCE S. DERMODY[2,3,4]*

Department of Biochemistry and Molecular Biology, Baylor College of Medicine, Houston, Texas 77030,[1] and Departments of Pediatrics[2] and Microbiology and Immunology[4] and Elizabeth B. Lamb Center for Pediatric Research,[3] Vanderbilt University School of Medicine, Nashville, Tennessee 37232

Received 20 November 2000/Accepted 13 April 2001

Reovirus virions are nonenveloped icosahedral particles consisting of two concentric protein shells, termed outer capsid and core. Outer-capsid protein σ1 is the viral attachment protein and binds carbohydrate molecules on the surface of host cells. Monoclonal antibody (MAb) 4F2, which is specific for outer-capsid protein σ3, blocks the binding of σ1 protein to sialic acid and inhibits reovirus-induced hemagglutination (HA). To determine whether MAb 4F2 inhibits HA by altering σ1-σ3 interactions or by steric hindrance, we analyzed the effect of 4F2 immunoglobulin G (IgG) and Fab fragments (Fabs) on HA induced by reovirus strain type 3 Dearing (T3D). The concentration of 4F2 IgG sufficient to inhibit T3D-induced HA was 12.5 μg per ml, whereas that of Fabs was >200 μg per ml. Dynamic light scattering analysis showed that at the concentration of IgG sufficient to inhibit HA, virion-antibody complexes were monodispersed and not aggregated. The affinity of 4F2 Fabs for T3D virions was only threefold less than that of intact IgG, which suggests that differences in HA inhibition titer exhibited by 4F2 IgG and Fabs are not attributable to differences in the affinity of these molecules for T3D virions. We used cryoelectron microscopy and three-dimensional image analysis to visualize T3D virions alone and in complex with either IgG or Fabs of MAb 4F2. IgG and Fabs bind the same site at the distal portion of σ3, and binding of IgG and Fabs induces identical conformational changes in outer-capsid proteins σ3 and μ1. These results suggest that MAb 4F2 inhibits reovirus binding to sialic acid by steric hindrance and provide insight into the conformational flexibility of reovirus outer-capsid proteins.

Mammalian reoviruses are nonenveloped, icosahedral viruses that contain a genome of 10 double-stranded RNA gene segments. Reovirus particles consist of an outer-capsid shell that surrounds a central core, which contains the viral genome. By cryoelectron microscopy (cryo-EM) and three-dimensional image analysis, virions of reovirus strain type 1 Lang (T1L) are ~850 Å in diameter and are notable for 600 finger-like projections, which correspond to the σ3 protein (14). The 600 copies of σ3 interdigitate with a more internal layer composed of 600 copies of μ1 protein. These proteins form the outer capsid. Large turrets composed of pentamers of λ2 protein are located at each of the icosahedral fivefold axes, and a small density at the center of each fivefold axis corresponds to viral attachment protein σ1.

The σ1 protein is comprised of an amino-terminal fibrous tail, which anchors the protein into the virion, and a compact, carboxy-terminal globular head (3, 8, 17, 19). Two discrete receptor-binding domains have been identified for reovirus strain type 3 Dearing (T3D) σ1. Sequences in the T3D σ1 head domain bind junction adhesion molecule (4), an integral tight junction protein expressed on epithelial and endothelial cells (28, 30). Sequences in the T3D σ1 tail domain bind sialic acid residues on glycosylated cell-surface molecules of erythrocytes and nucleated cells (9, 10, 13, 32, 35). Binding to sialic acid is required for the capacity of T3D to produce hemagglutination (HA) (1, 13, 20, 21, 33, 34) and to infect some types of cells in culture (10, 35). The σ1 protein in virions appears to assume a retracted conformation (14, 19), which might place it in a position where it could interact with σ3 (40).

As determined by X-ray crystallography, the σ3 protein is composed of two lobes organized around a central helix that spans the length of the protein (32a). The larger and more external lobe projects into the surrounding solvent. The smaller lobe interacts with the core-proximal outer-capsid protein, μ1 (14). During viral disassembly in cellular endosomes, the σ3 protein is removed from virions by acid-dependent proteolysis (2, 37), which is a requisite step in the penetration of reovirus into the cytoplasm (5, 22, 23, 29). Removal of σ3 during viral disassembly also is hypothesized to allow a change in the conformation of σ1 to a more extended form (32). Mutations in T3D σ3 determine the sensitivity of virions to proteolysis by the intestinal protease chymotrypsin (43) and the endocytic protease cathepsin L (16). Therefore, both σ1 and σ3 play important roles in reovirus entry into cells.

Monoclonal antibodies (MAbs) specific for each of the reovirus outer-capsid proteins have been isolated and characterized (6, 40). σ1-specific MAbs are serotype specific (6, 40), and some of these MAbs potently neutralize viral infectivity in plaque-reduction neutralization assays (6, 36, 40). Type 1 σ1-specific MAb 5C6 (40) and type 3 σ1-specific MAb 9BG5 (6) bind the σ1 head domain (9) and likely mediate neutralization

* Corresponding author. Mailing address for B. V. Venkataram Prasad: Department of Biochemistry and Molecular Biology, Baylor College of Medicine, One Baylor Plaza, Room N410, Houston, TX 77030-3498. Phone: (713) 798-5686. Fax: (713) 798-1625. E-mail: vprasad@bcm.tmc.edu. Mailing address for Terence S. Dermody: Elizabeth B. Lamb Center for Pediatric Research, Vanderbilt University School of Medicine, D-7235 MCN, Nashville, TN 37232-2581. Phone: (615) 322-2250. Fax: (615) 343-9723. E-mail: terry.dermody@mcmail.vanderbilt.edu.

by blocking access of σ1 to the head receptor on host cells. σ3-specific MAbs are not serotype specific (40) and are not capable of neutralizing viral infectivity (38). However, several σ3-specific MAbs are capable of inhibiting the σ1-mediated function of HA (40). The mechanism by which a σ3-specific MAb blocks the binding of σ1 to cell-surface sialic acid is not known.

In this study, we performed experiments to determine the mechanism by which σ3-specific MAb 4F2 inhibits the capacity of T3D to produce HA. We analyzed the effect of intact immunoglobulin G (IgG) and Fab fragments (Fabs) of MAb 4F2 on HA and aggregation of viral particles. We used cryo-EM and three-dimensional image reconstruction to visualize T3D virions, alone and in complex with either IgG or Fabs of MAb 4F2, to investigate whether conformational alterations in outer-capsid proteins are associated with the binding of 4F2 to σ3. The results indicate that IgG and Fabs of MAb 4F2 induce identical conformational alterations in the reovirus outer capsid, but only IgG is capable of inhibiting HA. At IgG concentrations sufficient to inhibit HA, viral particles are monodispersed, as assessed by dynamic light scattering (DLS) analysis. These findings provide strong evidence that σ3-specific MAb 4F2 inhibits σ1 binding to cell-surface sialic acid by steric hindrance.

MATERIALS AND METHODS

Cells, viruses, and antibodies. Murine L cells were grown in suspension culture in Joklik's modified Eagle's minimal essential medium (Irvine Scientific, Santa Ana, Calif.) supplemented to contain 5% fetal bovine serum (Intergen, Purchase, N.Y.), 2 mM L-glutamine, 100 U of penicillin per ml, 100 μg of streptomycin per ml, and 0.25 g of amphotericin per ml (Irvine). Reovirus strain T3D is a laboratory stock. Purified virion preparations were made using second-passage L-cell lysate stocks of twice-plaque-purified reovirus as previously described (19).

The σ3-specific MAb 4F2 (40), type 1 σ1-specific MAb 5C6 (40), and type 3 σ1-specific MAb 9BG5 (6) were purified from hybridoma cell supernatants by protein A column chromatography (National Cell Culture Center, Cellex Biosciences, Inc., Minneapolis, Minn.). Biotinylated 4F2 was generated by incubating 2 mg of MAb 4F2 per ml with sulfo-*N*-hydroxysuccinimide-biotin (Pierce, Rockford, III.), at 0.14 mg per ml (final concentration) with antibody, at room temperature for 2 h. Biotinylated 4F2 was dialyzed extensively against phosphate-buffered saline (PBS), and the concentration of the biotinylated antibody was determined using the Bio-Rad *DC* protein assay (Bio-Rad Laboratories, Hercules, Calif.).

Generation of Fabs of σ3-specific MAb 4F2. Fabs of MAb 4F2 were generated using an ImmunoPure Fab purification kit (Pierce). IgG molecules of MAb 4F2 were concentrated to approximately 5 mg per ml in PBS and digested with 83 μg of papain per ml (2.3 BAEE units per ml) in a total volume of 1.5 ml. Fabs were recovered by protein A column chromatography, dialyzed against PBS, and concentrated by Centricon (Millipore Corporation, Bedford, Mass.) centrifugation. Concentrations of IgG and Fabs of MAb 4F2 were determined by the Bio-Rad *DC* protein assay.

HAI Assays. Purified T3D virions (4 HA units [10^{11} particles]) in a volume of 25 μl in PBS were incubated with 0 to 200 μg of IgG or Fabs of MAb 4F2, 5C6, or 9BG5 per ml in a volume of 25 μl in PBS at 37°C for 1 h in 96-well round-bottom microtiter plates (Corning-Costar, Cambridge, Mass.). Human type A erythrocytes were washed twice with PBS and resuspended at a concentration of 2% (vol/vol). Erythrocytes (50 μl) were added to the virion-antibody mixtures, and plates were incubated at 4°C overnight. The HA inhibition (HAI) titer was defined as the lowest concentration of antibody capable of inhibiting HA.

Affinity of IgG or Fabs of σ3-specific MAb 4F2 for T3D virions. Enzyme immunoassay-radio immunoassay 96-well plates (Corning-Costar) were coated with 100 μl of purified virions per well of reovirus T3D at 10^{12} particles per ml in carbonate-bicarbonate coating buffer (Sigma, St. Louis, Mo.) and incubated at room temperature for 1 h. Coated plates were washed four times with PBS containing 0.05% Tween 20 detergent (PBS-T) and stored at 4°C until use. A saturation curve was determined for the binding of biotinylated 4F2 to T3D virions. Biotinylated 4F2 (0.0005 to 50 μg per ml) was added to virion-coated wells at 100 μl per well, and plates were incubated with rocking at room temperature for 30 min. Wells were washed four times with PBS-T to remove unbound biotinylated 4F2. Avidin-biotinylated horseradish peroxidase complex (ABC) reagent (Vector Laboratories, Burlingame, Calif.) was prepared according to the manufacturer's instructions. ABC reagent was added at 100 μl per well and incubated with rocking at room temperature for 30 min. Wells were washed four times with PBS-T to remove unbound ABC reagent. One 10 mg 2,2′-azinobis(3-ethylbenzthiazoline-6-sulfonic acid) (ABTS) tablet was dissolved in 100 ml of 0.05 M phosphate-citrate buffer (Sigma), and 30% H_2O_2 was added just prior to use (2.5 μl per 10 ml). ABTS-H_2O_2 substrate was added at 100 μl per well and incubated without rocking at room temperature in the dark for 10 min, followed by measurement of absorbance at 405 nm. The concentration of biotinylated 4F2 resulting in 50% saturation (0.5 μg per ml) was used in competition assays in which various concentrations of unbiotinylated IgG and Fabs of MAb 4F2 were used to compete the binding of biotinylated 4F2 to T3D virions. Competition assays were performed using a 1:2 dilution of ABC reagent, and virion-antibody mixtures were incubated with ABC reagent for 15 min.

Preparation of virion-antibody complexes for cryo-EM. Virions of reovirus T3D (10^{13} per ml) were incubated with either IgG or Fabs of MAb 4F2 at a ratio of five antibody molecules for each σ3 protein (600 copies per virion). Samples were incubated at room temperature for 2 h followed by overnight at 4°C and were examined by negative-stain electron microscopy to assess particle concentration and estimate antibody binding. Samples then were frozen for cryo-EM.

DLS. Virions were incubated with 4F2 IgG at the same concentrations used in the HAI assays. After incubation at 37°C for 1 h, samples were analyzed for DLS using a DynaPro-801 (Protein Solutions, Inc., Charlottesville, Va.) to determine the dispersion characteristics of the particles.

Cryo-EM. Specimen preparation for cryo-EM was performed using standard procedures (15). A 4-μl aliquot of each specimen (virions, 4F2 IgG-virion complexes, or 4F2 Fab-virion complexes) was applied to one side of a holey carbon grid. The grid was then blotted and plunged into a bath of liquid ethane (−180°C). The frozen-hydrated sample was transferred to a pre-cooled GATAN cryoholder (GATAN, Inc., Pleasanton, Calif.) and imaged using a JEOL 1200 transmission electron microscope (JEOL USA, Inc., Peabody, Mass.), operated at 100 kV and maintained at a specimen temperature of −163°C. Regions of interest were imaged at ×30,000 magnification with an electron dose of 5 electrons/Å^2. From each region, a focal pair was recorded with intended defocus values of 1 and 2 μm. The electron images were recorded with a 1-s exposure on Kodak SO-163 film (Kodak, Rochester, N.Y.). Film was developed in Kodak D-19 developer at 21°C for 12 min and fixed in Kodak fixer at 21°C for 10 min.

Three-dimensional image reconstructions. Micrographs were selected based on particle concentration, quality of ice, and appropriate defocus conditions. Images were digitized on a Zeiss SCAI microdensitometer (Carl Zeiss, Inc., Englewood, Colo.), using a 7-μm step size. Pixels were averaged to give a 14-μm step size that corresponded to 4.67 Å per pixel in the object. Particles were boxed with an area of 256 by 256 pixels. Determination of orientational parameters, refinement of these parameters, and three-dimensional reconstructions were performed using the ICOS Toolkit software suite (27). Orientations of the particles were determined using the common lines approach (11) and refined by the cross-common lines method (18). Three-dimensional image reconstructions from a set of particles that adequately represented the icosahedral asymmetric unit were computed by cylindrical expansion methods (11). The further-from-focus micrograph in each focal pair was processed first to obtain a low-resolution reconstruction. This reconstruction then was used to determine correct orientations for particles imaged in the corresponding closer-to-focus micrograph.

Image reconstructions were computed to a resolution within the first zero of the contrast transfer function (CTF) of the corresponding micrograph. Defocus values were determined from CTF ring positions in the sum-of-particle Fourier transforms. Defocus values of various specimens in the closer-to-focus micrographs ranged from 1.2 to 1.4 μm. Image reconstructions were corrected for the effects of the CTF using previously described procedures (46). Final resolution for each reconstruction was determined by Fourier ring correlation analysis (39). Image reconstructions were computed to ~23-Å resolution for comparative analysis. Contour levels in each reconstruction were chosen to represent equal volumes between radii at ~305 Å and at ~425 Å. Reconstructions were viewed on a Silicon Graphics workstation (SGI, Mountain View, Calif.) using IRIS Explorer version 3.5 software (Numerical Algorithms Group, Inc., Oxford, United Kingdom).

Fitting of X-ray structures into the cryo-EM reconstructions. The X-ray coordinates for σ3 (32a) and representative Fab, 1clz (24), were initially rigid-body fitted into their respective portions of the cryo-EM density maps by visual

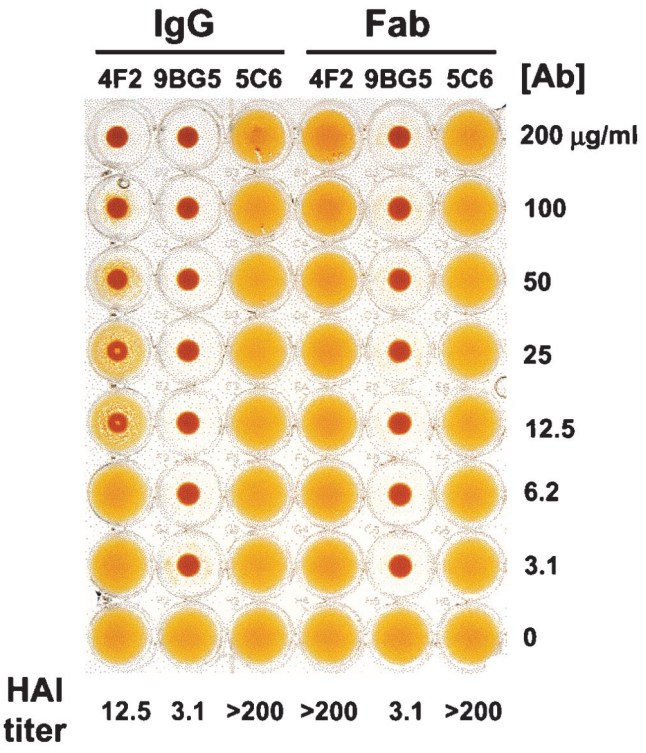

FIG. 1. HAI capacity of σ3-specific MAb 4F2 IgG and Fabs. T3D virions (4 HA units [10^{11} particles]) were incubated with IgG and Fabs of MAb 4F2, 9BG5, or 5C6 at the concentrations shown at 37°C for 1 h. Human type A erythrocytes were added, and plates were incubated at 4°C overnight. The HAI titer for each antibody was defined as the lowest concentration of antibody capable of inhibiting HA. The experiment was performed in triplicate. Shown is a representative experiment.

inspection using the graphical program O (25). Subsequent refinements were performed using the Situs program package, a rigid-body correlation fitting procedure that allows the fitting of X-ray structures into low-resolution cryo-EM density maps (45). The fully refined positions of σ3 and Fab were displayed using Ribbons version 2.85 software (7).

RESULTS

Fabs of MAb 4F2 do not inhibit HA by T3D virions. The σ3-specific MAb 4F2 is capable of inhibiting HA by reovirus strain T3D (40). To determine whether Fabs of MAb 4F2 are capable of inhibiting T3D-induced HA, HAI assays were performed using 4F2 IgG and Fabs. Type 3 σ1-specific MAb 9BG5 and type 1 σ1-specific MAb 5C6 were used as isotype-matched specificity controls. IgG molecules of MAb 9BG5 are capable of inhibiting HA by T3D, whereas those of MAb 5C6 are not (40). T3D virions were incubated with increasing concentrations of IgG and Fabs of each antibody and tested for the capacity to produce HA (Fig. 1). 4F2 IgG inhibited HA at all concentrations of ≥12.5 μg per ml. In contrast, 4F2 Fabs did not inhibit HA at concentrations of ≤200 μg per ml, which was the highest concentration of antibody tested. Therefore, the HAI titer for 4F2 IgG was at least 16-fold lower than that for 4F2 Fabs. HAI titers for 9BG5 Fabs were equivalent to those of intact IgG, and both IgG and Fabs of MAb 5C6 did not produce HAI at any concentration of antibody used. These results indicate that, unlike IgG, Fabs of MAb 4F2 do not interfere with the binding of T3D to erythrocytes.

IgG and Fabs of MAb 4F2 bind T3D virions with similar affinity. To determine whether differences in the capacity of IgG and Fabs of MAb 4F2 to inhibit T3D-induced HA are associated with differences in their affinity for virions, we tested the capacity of each to bind T3D virions by using an indirect enzyme-linked immunosorbent competition assay. Purified T3D virions were coated onto 96-well plates, and then biotinylated 4F2 IgG was added. Increasing concentrations of unbiotinylated 4F2 IgG and Fabs were used to compete the binding of biotinylated 4F2 to T3D virions, and an avidin-biotin-conjugated enzyme detection method was used to quantitate bound biotinylated 4F2 after competition (Fig. 2). Results from three independent experiments showed that 4F2 IgG and Fabs bound T3D virions with similar affinity. At lower concentrations (between 0 and 0.01 μM), IgG and Fabs did not compete the binding of biotinylated 4F2 to T3D. At higher concentrations (between 0.01 and 1 μM), both IgG and Fabs competed the binding of biotinylated 4F2 in a dose-dependent manner. The concentration of IgG required to compete 50% of the binding of biotinylated IgG to T3D was 0.07 μM, whereas that of Fabs was 0.4 μM, or approximately sixfold more. These results indicate that differences in HAI exhibited by 4F2 IgG and Fabs are not attributable to differences in their binding affinity for virions.

4F2 IgG does not produce aggregation of reovirus virions. To determine whether MAb 4F2 mediates HAI by producing aggregation of viral particles, we used DLS to analyze T3D virions alone and in complex with MAb 4F2. At the minimum concentration of 4F2 IgG sufficient to inhibit HA (12.5 μg per ml), individual virion-antibody complexes were found to be monodispersed and consistent with the size of virion-antibody complexes as determined by cryo-EM (data not shown). DLS analysis of Fab-bound virions also demonstrated monodispersed virion-antibody complexes, albeit of a slightly smaller

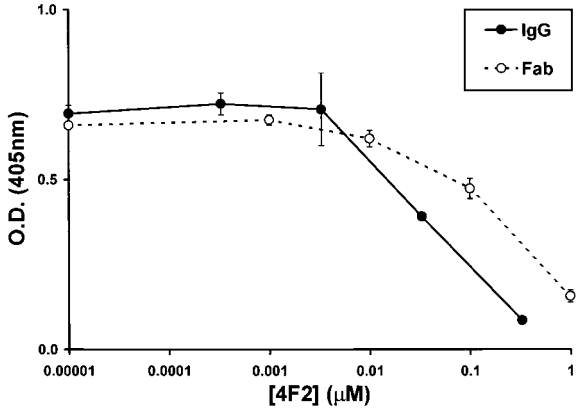

FIG. 2. Affinity of σ3-specific MAb 4F2 IgG and Fabs for T3D virions. Biotinylated 4F2 IgG (0.5 μg per ml) was bound to T3D-coated plates. Unbiotinylated 4F2 IgG and Fabs at the concentrations shown were used to compete the binding of biotinylated 4F2 to T3D virions. The amount of biotinylated 4F2 bound in the presence of competitor is indicated by absorbance at 405 nm. Error bars represent standard error of the mean for three independent experiments. O.D., optical density.

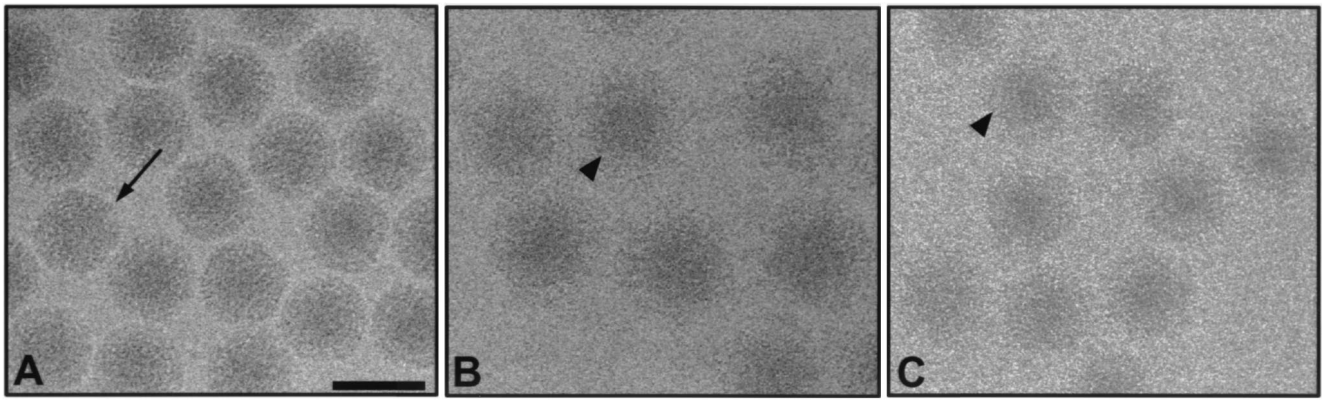

FIG. 3. Cryo-EM images of frozen-hydrated virions of reovirus T3D. (A) Native virions. An arrow indicates projections of σ3 on the outer capsid. (B) Virions bound by 4F2 IgG. An arrowhead indicates mass density due to IgG. (C) Virions bound by 4F2 Fabs. An arrowhead indicates mass density due to Fabs. All images were obtained at ×30,000 magnification using an electron dose of 5 electrons/Å^2. Scale bar, 1,000 Å.

size consistent with the absence of Fc domains in the antibody molecules. These results strongly suggest that MAb 4F2 does not mediate HAI by antibody-induced aggregation of viral particles.

Cryo-EM of native virions and antibody-bound virions. To determine whether differences in the capacity of 4F2 IgG and Fabs to inhibit HA by T3D are due to antibody-induced alterations in the conformation of viral outer-capsid proteins, we used cryo-EM and three-dimensional image analysis to compare the structures of native virions and virions bound by either intact IgG or Fabs. Cryo-images of unstained frozen-hydrated native virions (Fig. 3A), IgG-bound virions (Fig. 3B), and Fab-bound virions (Fig. 3C) were collected at ×30,000 magnification. Native virion particles and virion-antibody complexes were randomly oriented within a thin layer of vitreous ice. Finger-like projections corresponding to σ3 protein were observed in the native virion structures. Due to the number of σ3 molecules on the surface of the virion (600 copies [14]) and the affinity of MAb 4F2 for σ3 protein (40), the σ3 projections were completely obscured after incubation of virions with either IgG or Fabs of MAb 4F2. Both forms of antibody produced a halo of density surrounding the virion structures. Incubation of virions with either IgG or Fabs of MAb 4F2 resulted in an approximately 26 or 19% increase in particle diameter, respectively, compared to the diameter of native virions. This increase in diameter rendered antibody-bound virions easily distinguishable from unbound virions. Native and antibody-bound virions were digitally extracted from each micrograph and used for image reconstructions. Inverse eigenvalues for 95% of the particles were below 0.1, indicating adequate sampling for the computed resolutions.

Structures of IgG-bound and Fab-bound virions. Isosurface image reconstructions of native T3D virions (computed to 23-Å resolution using 183 particles), IgG-bound virions (computed to 26-Å resolution using 49 particles), and Fab-bound virions (computed to 23-Å resolution using 220 particles) are shown in Fig. 4A to C, respectively. In contrast to the cryo-images of native and Fab-bound virions, there were fewer particles observed in the cryo-images of IgG-bound virions, although the viral particle concentration was equivalent in each case. The apparent discrepancy in particle number might be attributable to either a change in the surface properties of the IgG-bound virions or loss of virion-antibody complexes during cryo-specimen preparation. As a result, fewer particles were used in the image reconstruction of IgG-bound virions. The IgG-bound virion has a larger diameter than the Fab-bound virion due to the Fc portion of the antibody. However, at the radius corresponding to the antibody Fc fragment, the mass density is not well resolved in the reconstruction. Therefore, data beyond a radius of 480 Å were removed in both the IgG-bound and Fab-bound virion reconstructions to reveal density due only to the Fab portion of the antibody. The IgG-bound and Fab-bound virions have similar patterns of antibody attachment to σ3 protein. Individual Fabs could not be visualized but instead formed continuous rings of mass density surrounding each of the local threefold axes. However, at the fivefold axes, bilobed structures bound to the distal tips of the σ3 protein were clearly resolved. These σ3-binding structures appeared to be of the correct size and shape of Fabs.

Placement of the σ3 structure into native and Fab-bound virion density maps. The X-ray coordinates of σ3 protein (32a) were manually placed into four projections of σ3 in the native virion density adjacent to a fivefold axis (Fig. 5A and B). The projections are designated 1 through 4 in Fig. 5A to indicate position relative to the fivefold axis. The density corresponding to each projection was extracted separately from both native virions and Fab-bound virions. The initial fitting indicated that the σ3 structure could be placed into the cryo-EM density in two different orientations related by a 180° rotation around the long axis of the molecule. We used a quantitative method to refine the placement of the σ3 structure in native and Fab-bound densities. The manually placed coordinates were rigid-body fitted using the Situs program package, which produces placement of multiple orientations with a score. In the native virion density, the four σ3 molecules were fitted individually with an average cross-correlation coefficient of 0.78. The inverted fitting of the σ3 protein gave a cross-correlation coefficient of 0.70. The orientation that provided the higher cross-correlation coefficient is in agreement with that previously reported (32a) (Fig. 5C). The larger of the two σ3 lobes (residues 91 to 286 and 337 to 365) is distal to the surface of the virion and contains a region of α-helix that protrudes away from the virion particle. The smaller lobe (residues 1 to 90 and

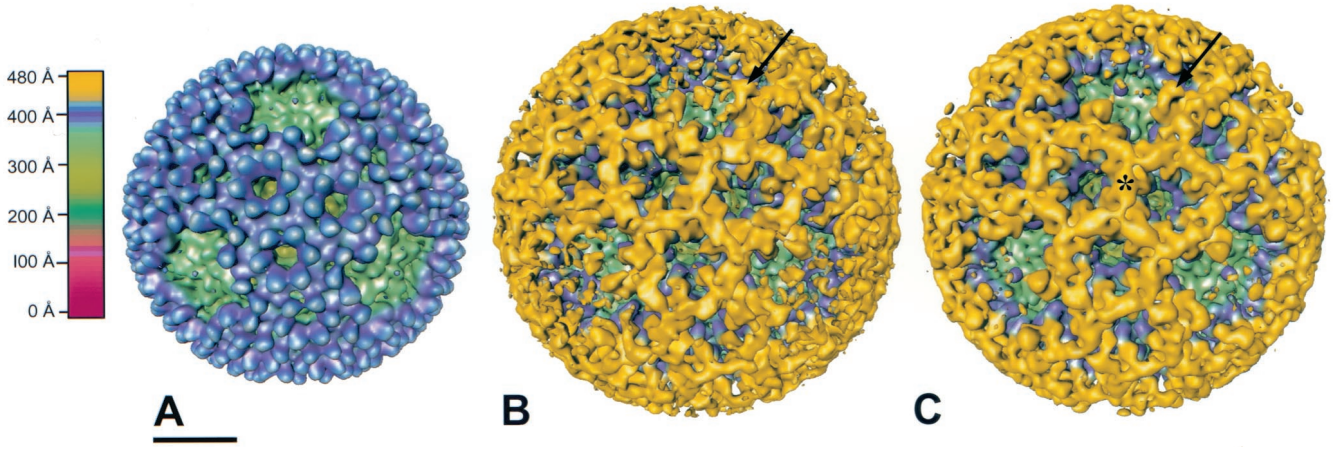

FIG. 4. Surface-shaded representations of native T3D virions (A), T3D virions bound by 4F2 IgG (B), and T3D virions bound by 4F2 Fabs (C) viewed along an icosahedral threefold axis. The capsids are radially depth-cued as shown in the color chart. The same coloring scheme is used in other figures unless indicated otherwise. (A) Projections of σ3 (blue) protrude from the surface of the virion. A λ2 turret lies in a depression at each of the fivefold axes (green). (B) Mass density due to IgG bound to σ3 is shown in yellow. The IgG-bound virion structure has been radially cut at ~480 Å to reveal only the Fab portion of the antibody. An arrow indicates a complete Fab. (C) Mass density due to Fabs bound to σ3 is shown in yellow. Fabs extend distally to a radius of ~480 Å and form continuous tubes of density (*) that surround the channels made by σ3. Entire Fabs are observed overhanging the fivefold axes (arrow). Scale bar, 200 Å.

287 to 336) is more virion proximal and interacts with the underlying μ1 protein layer.

Placement of σ3 into the native density was next examined for the quality of fit into the σ3 density of Fab-bound virions. For each of the four projections of σ3 examined, the σ3 molecules in Fab-bound virions are in slightly different conformations but are oriented similarly to native virions (data not shown). At the resolution of the reconstructions obtained in this study, it was not possible to determine whether the entire σ3 molecule moves as a single unit, or whether small confor-

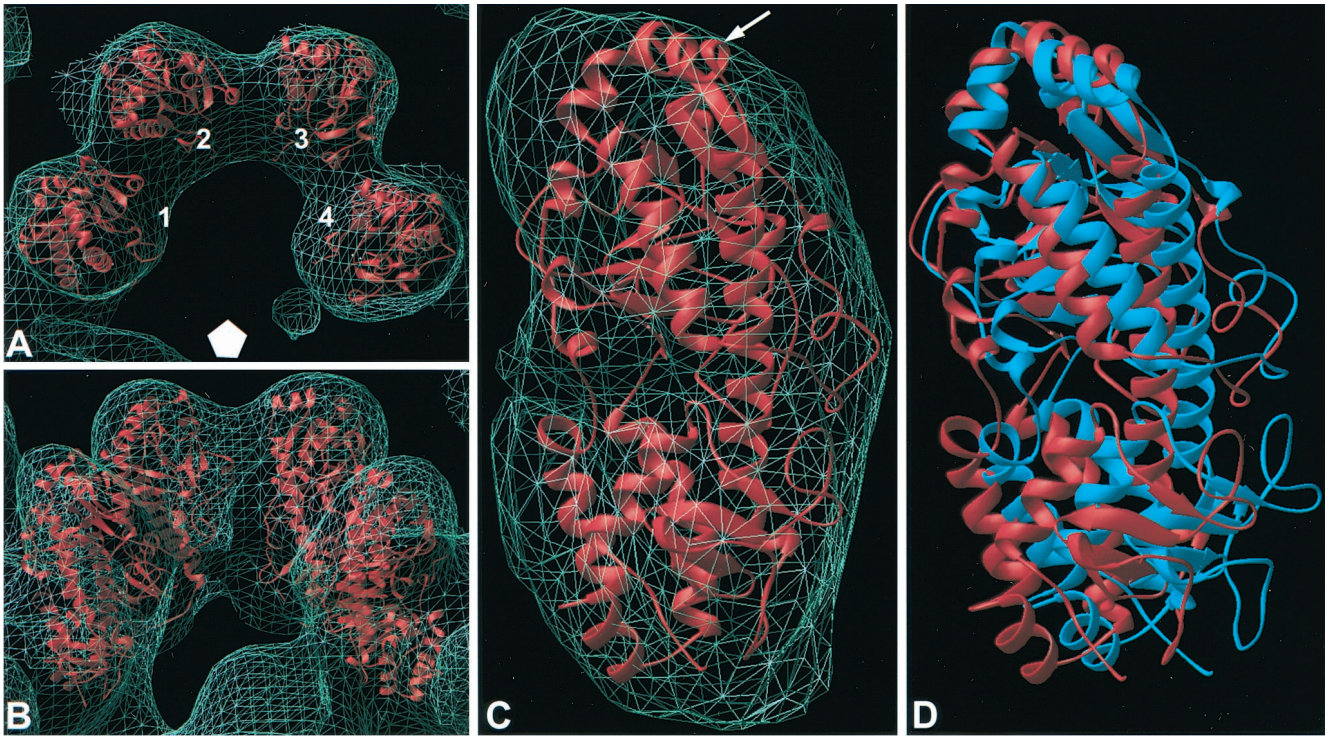

FIG. 5. Placement of the X-ray structure of σ3 into the cryo-EM reconstruction density of both native and Fab-bound virions. The σ3 coordinates placed individually into four projection densities of native virions are displayed from above (A) and from the side (B). Numbers 1 to 4 indicate σ3 positions relative to the general location of the adjacent fivefold axis (white pentagon). (C) Placement of σ3 into a single projection density of the native virion. An arrow indicates the location of an α-helix containing amino acid 116. (D) Placement of σ3 into position 1 of both native virions (red) and Fab-bound virions (blue).

mational changes occur once Fabs have bound. The σ3 coordinates were rigid-body fitted into the Fab-bound virion density using the Situs program package. The four projections were fitted with an average cross-correlation coefficient of 0.70. In comparison to the fitting of σ3 in native virions, small alterations in positions 1 and 4 and larger alterations in positions 2 and 3 were observed in the fitting of σ3 in Fab-bound virions (data not shown). After binding of 4F2 Fabs, the σ3 in position 1 rotates outward and away from the group of four projections. σ3 structures placed into position 1 of both native virions and Fab-bound virions are shown in Fig. 5D. These results indicate that the conformation of σ3 in Fab-bound virions is altered in comparison to native virions, presumably as a consequence of antibody binding.

Orientation of Fabs of MAb 4F2 bound to T3D σ3 protein. Densities of Fabs at the fivefold axes correlated well with the expected envelope of an Fab molecule. There are two lobes in an Fab: the variable domain, which binds antigen, and the constant domain, which is more distal to the antigen-binding epitope (12). The general structure of an Fab is highly conserved. However, the elbow angle between the constant and variable domains can vary, as can the loops of the antibody paratope that form the complementary-determining region (CDR). To determine the position and orientation of 4F2 Fabs bound to σ3 protein, we used the X-ray coordinates of the 1clz Fab (24) as a prototype to fit into the reconstruction of antibody-bound virions. Atomic coordinates of the 1clz Fab fragment were first manually placed into the cryo-EM reconstruction of the Fab-bound virions. The fitting was refined using the Situs program package, which gave a cross-correlation coefficient of 0.66. Both the variable and constant domains of the Fab were fitted unambiguously into the cryo-EM reconstruction of the Fab-bound virion (Fig. 6, top). The CDR loops of the fitted Fab were in close proximity to a virion-distal α-helix, which contains amino acid 116. This amino acid lies directly beneath the bound Fab and is in close (~5 Å) contact with the fitted Fab coordinates. Comparative sequence analysis of σ3 in reovirus strains that differ in the capacity to be bound by MAb 4F2 implicated residue 116 as important for the binding of 4F2 to σ3 (26).

When the Fab coordinates were superimposed onto the IgG-bound virion density in the same orientation as in the Fab-bound virion density, only the variable portion was positioned within the mass density (data not shown). The constant domain could be positioned into the IgG-bound density only by manually altering the elbow angle of the Fab (data not shown). This finding suggests that the Fab portion of MAb 4F2 bound to T3D has a different elbow angle when in monovalent or bivalent forms. However, the Fab variable domain in both the IgG-bound and Fab-bound virion structures retains the same orientation and therefore contacts the σ3 protein at the same site.

At locations in the Fab-virion reconstruction other than in the immediate vicinity of the fivefold axes, it was more difficult to accurately position the Fab structure in the cryo-EM density. In an attempt to evaluate the percent occupancy of Fabs bound to T3D, we placed the Fab coordinates into the cryo-EM density at the hexameric locations around an icosahedral threefold axis in such a way as to account for the continuous tubes of antibody density (data not shown). This analysis suggests that Fabs are bound at an angle to the surface of σ3 and that the sides of each Fab come into close contact with neighboring Fabs. If a very tight, antiparallel packing arrangement is assumed, Fabs were determined to be capable of packing into the density with full occupancy.

Conformational changes close to the σ3 protein and Fab variable domain interface. To determine whether the binding of IgG and Fabs of MAb 4F2 to T3D virions results in conformational changes in viral outer-capsid proteins, we analyzed cross sections of the native and antibody-bound virion reconstructions at various radii. Radial sections of antibody-bound virions near the top of the σ3 protein, at a radius of ~407 Å, revealed a conformational change compared with native virions. In native virions, σ3 proteins surrounding local sixfold axes are attached to their neighbors, forming hexameric rings (Fig. 7A). However, in the IgG-bound and Fab-bound virions, the hexameric rings are broken, and individual σ3 proteins are distinct and separated from each other (Fig. 7B and C). Binding of 4F2 IgG and Fabs to T3D also resulted in conformational changes that are transferred well beneath the paratope-epitope interface. A small but noticeable conformational change was observed in the antibody-bound virions beneath the σ3 layer. At a radius of ~385 Å, which is within the μ1 layer (14), antibody-bound virions contain a spur of density that projects into a hole formed at the center of the hexameric ring of μ1 proteins (Fig. 7E and F). This feature was consistent throughout various contour levels and was visualized in independent reconstructions of IgG-bound and Fab-bound virions. In native virions, no such density was observed (Fig. 7D). Therefore, the binding of σ3-specific MAb 4F2 to T3D virions induces conformational alterations both in the σ3 layer and in the more internal μ1 layer of the virion outer capsid.

DISCUSSION

Studies of mechanisms by which antiviral antibodies inhibit viral infectivity can yield an improved understanding of virus structure and replication. Antibodies can neutralize viruses by blocking viral binding to cell-surface receptors or cross-linking viral particles, thereby reducing the number of infectious units (44). Antiviral antibodies also can inhibit intracellular steps in viral replication, such as internalization and disassembly (41). MAb 4F2, which is specific for the reovirus σ3 protein (40), inhibits the capacity of reovirus to produce HA (40), which is a property mediated by the σ1 protein (6, 13, 31, 34, 42). This finding indicates that some virus-specific MAbs block functions of proteins other than those to which they bind (40). We conducted experiments to determine mechanisms by which a σ3-specific MAb inhibits a σ1 function. We assessed the capacity of IgG and Fabs of MAb 4F2 to (i) inhibit HA by T3D, (ii) produce aggregation of viral particles, and (iii) mediate conformational alterations of viral outer-capsid proteins. We found that IgG and Fabs induce identical conformational changes in σ3 and that neither produces particle aggregation. However, 4F2 IgG molecules inhibit HA, whereas Fabs do not. These results are most consistent with a steric hindrance mechanism of MAb 4F2 action.

The concentration of IgG required to inhibit T3D-induced HA was at least 16-fold less than that of Fabs, which were not capable of HAI even at the highest concentration tested. This finding is not explained by differences in the affinity of 4F2 IgG

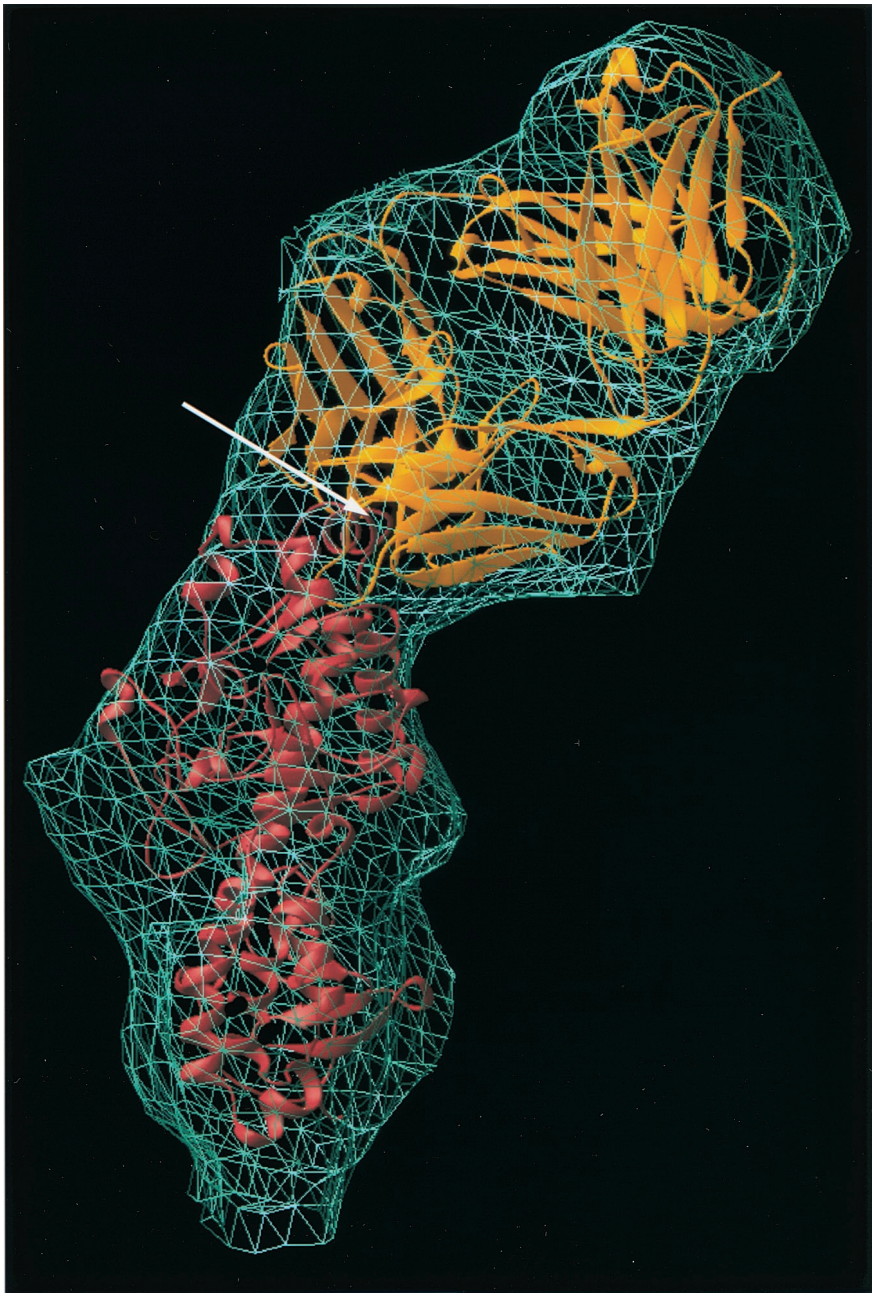

FIG. 6. Placement of the X-ray structures of both Fab (top) and σ3 (bottom) into the cryo-EM reconstruction density of Fab-bound virions (mesh). The atomic coordinates of Fab and σ3 were placed using the Situs program package and displayed in Ribbons in gold and red, respectively. The location of amino acid 116 is indicated by an arrow.

and Fabs for T3D virions. The concentration of Fabs required to compete 50% of the binding of IgG to T3D was approximately sixfold greater than that of IgG. However, since Fabs contain one binding site and IgG contains two binding sites, the concentration of Fabs required to compete IgG binding might be expected to be twice that of IgG. Therefore, the actual difference in affinity of IgG and Fabs of MAb 4F2 for T3D virions is approximately threefold. Since 4F2 Fabs did not inhibit HA at the highest concentration used in these experiments, it is possible that Fabs are actually incapable of preventing T3D-induced HA at any concentration. This conclusion seems likely since image reconstructions of Fab-bound virions indicate almost complete occupancy of 4F2-binding sites at a concentration of Fabs less than that used in the experiments to inhibit HA.

IgG and Fabs of 4F2 bound the same site on σ3 in the image reconstructions of IgG-bound and Fab-bound virions. 4F2 IgG and Fabs that bind to hexameric rings of σ3 protein, around the icosahedral threefold axes, are packed tightly together. These Fabs are bound at an angle tangential to the virion surface, which results in neighboring Fabs coming into close contact with each other. Such a close association of σ3-bound

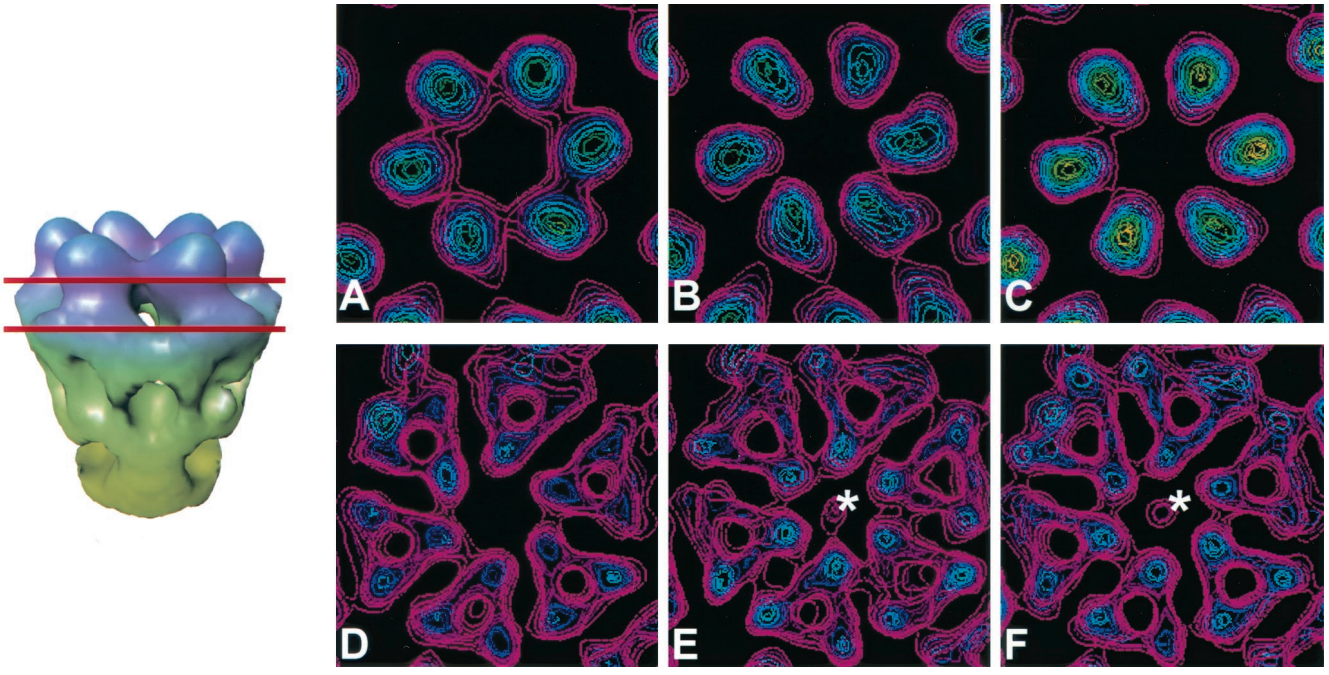

FIG. 7. Antibody-induced structural changes in the virion. Sections (14-Å thick) through the σ3 protein layer (top row) at a radius of ~407 Å and through the μ1 protein layer (bottom row) at a radius of ~385 Å are displayed for each reconstruction. Red lines indicate the locations of these sections on a side view of a conical cutaway of the hexameric arrangement of σ3 and μ1 in native virions. In native virions (A), σ3 subunits appear to be in contact with each other, whereas in the IgG-bound virions (B) and Fab-bound virions (C), the σ3 subunits are more distinct. In native virions, an unobstructed channel is observed traversing the μ1 layer (D). However, in IgG-bound virions (E) and Fab-bound virions (F), a small density is present at the center of the hexameric arrangement of μ1 proteins (*).

Fabs makes it difficult to visualize individual Fab molecules at the resolution obtained in this study. In contrast, individual Fabs are clearly observed in the incomplete hexameric rings, which surround the fivefold axes, presumably due to fewer σ3 proteins at these locations (four versus six), with resultant decreased crowding of bound antibodies.

Our analysis of IgG-bound and Fab-bound virion structures indicates that at the fivefold axes, the orientation of the Fab variable domain onto the σ3 protein is identical to that of the variable domain of IgG. This was not unexpected, since the interaction between the variable domain and the protein epitope is not affected by cleavage of intact IgG into Fabs (12). However, the location of the constant domain of the Fab was not the same in the IgG-bound and Fab-bound virion structures. In IgG-bound virions, the elbow angle of the Fab is altered in comparison to Fab-bound virions. The elbow region of Fabs is known to be flexible (12); therefore, it is possible that the presence of Fc and the other Fab in the intact IgG necessitates a small change in the elbow angle of the bound Fab for an optimal interaction with the virion. Torsional alterations also can be accommodated at the hinge region of the antibody, which is where two Fabs connect the Fc portion (12). The Fc and the unbound Fab portions are not resolved in our reconstructions, indicating that the orientations of these two portions vary considerably among the bound IgG molecules.

Conformational changes caused by the binding of IgG and Fabs are identical, and the most significant changes from the native virion structure are observed in the σ3 and μ1 layers. After IgG or Fab binding, the σ3 proteins no longer form continuous hexameric rings of density but are separated from each other. It is possible that in order to bind MAb 4F2, the σ3 proteins must separate slightly. The magnitude of these movements is likely to be limited by neighboring hexameric units of σ3. A conformational change in the μ1 layer of antibody-bound virions results in a spur of density protruding into the hexameric ring of μ1 proteins. Although it is likely that this density belongs to μ1, we cannot rule out the possibility that it could originate from one of the core proteins. A similar density was seen in a reconstruction of virions of reovirus strain T1L in the absence of antibody binding (14). This result is in contrast to the image reconstructions of native T3D virions obtained in this study, which suggests that a strain-specific polymorphism exists in the appearance of a central density in the hexameric arrangement of μ1 proteins. Nonetheless, our findings show that antibody binding to the viral surface can induce conformational changes well beneath the antibody-protein interface.

Since the binding of IgG and Fabs of MAb 4F2 to σ3 protein induces identical conformational changes in the virus structure, the differences in HAI capacity of 4F2 IgG and Fabs cannot be attributed to structural alterations caused by these molecules. We thought it possible that aggregation of IgG-bound particles might contribute to the inhibition of HA by limiting access of σ1 to cell-surface sialic acid. However, cryo-EM images of the IgG-bound virions show many well-decorated particles that are clearly separated from neighboring virions. Furthermore, at the concentration of 4F2 IgG sufficient to inhibit HA, virion-antibody complexes were well dispersed, as assessed by DLS experiments. These results exclude the possibility that 4F2-mediated HAI is due to either alteration in σ1-σ3 interactions or aggregation of IgG-bound viri-

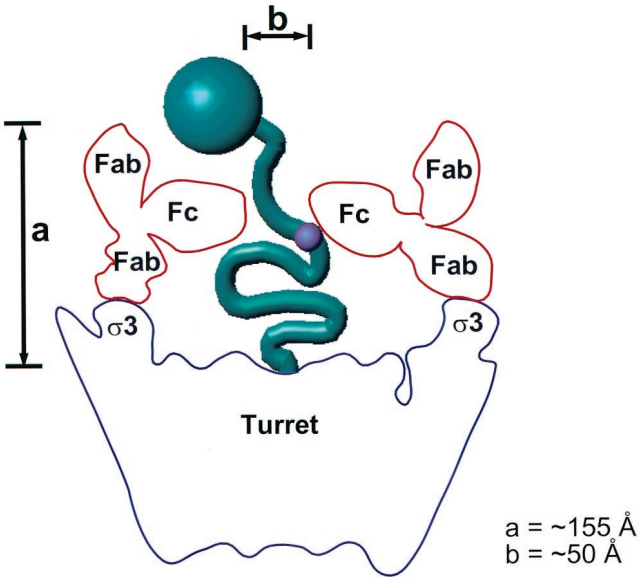

FIG. 8. A model for inhibition of HA by MAb 4F2. The maximum height (indicated by a) of an intact IgG, considering the conformational flexibility between the Fc and the Fab portions, is ~155 Å. Constraining one of the Fab arms of an intact antibody (red) to superimpose onto the fitted Fab positions the Fc portion of the antibody almost horizontally across the turret (blue). In this position, the fivefold-related Fc portions would leave a gap (indicated by b) of ~50 Å, which would sterically hinder access of the σ1 sialic acid-binding domain (small purple circle) to cell-surface sialic acid but not that of the σ1 head domain (large green circle) to its receptor.

ons. Instead, our data provide strong evidence that MAb 4F2 inhibits HA by steric hindrance of σ1-sialic acid interactions.

How does a σ3-specific MAb sterically hinder the capacity of σ1 to bind cell-surface sialic acid? We propose a model for the possible position of the unbound Fab arms and the Fc portions of MAb 4F2 bound to virions that is consistent with a steric hindrance mechanism of HAI (Fig. 8). When the X-ray structure of the Fab portion of an entire IgG is superimposed onto the fitted Fab, the Fc portion of the antibody would lie almost parallel to the λ2 turret and the unbound Fab arm would likely project radially away from the viral particle. The Fc portions of bound IgG molecules would not entirely close the turret but would leave a gap of ~50 Å at the center. The maximum height of intact IgG from the base of the turret, considering possible conformational flexibility of the Fab and Fc portions of the molecule, would be ~155 Å. In its fully extended conformation, purified σ1 is ~480 Å in length (17). The domain in T3D σ1 that binds sialic acid is located in the fibrous tail (9, 10, 13), ~225 Å from the virion-proximal base (10, 17). If virion-associated σ1 were in an extended conformation, neither Fabs nor IgG molecules would be expected to hinder access to this site, and neither should inhibit HA activity. However, 4F2 IgG molecules but not Fabs inhibit HA. Hence, our findings are in agreement with previous observations that σ1 is not fully extended when bound to virions (14, 19). The Fc portions that are postulated to project horizontally above the turret would likely mask the σ1 sialic acid-binding domain but not the head-receptor-binding domain since 4F2 IgG molecules do not neutralize viral infectivity (38). In Fab-bound virions, the top of the turret is more accessible, and we propose that σ1 can still interact with cell-surface sialic acid after Fab binding. Therefore, we conclude that HA inhibition by 4F2 is most likely due to steric hindrance of the σ1 sialic acid-binding domain by the Fc portion of intact IgG.

The cross-correlation fitting using the Situs program package provided an optimal placement of the X-ray coordinates for both the σ3 protein and an Fab molecule into their respective densities in the image reconstruction of Fab-bound virions. Examination of the σ3 and Fab X-ray coordinates fitted into the Fab-bound virion reconstruction allowed us to define the 4F2 epitope, which contains an α-helix of σ3 that is positioned almost parallel to the surface of the virus. This helix includes amino acid 116, which has been shown to influence the capacity of MAb 4F2 to bind reovirus field isolate strains (26).

Results reported here indicate that the binding of reovirus outer-capsid protein σ3 by MAb 4F2 inhibits HA induced by T3D σ1 protein through steric hindrance and that antibody binding of σ3 results in conformational changes in both the σ3 and μ1 protein layers of the reovirus outer capsid. Further insight into mechanisms by which antibodies are capable of inhibiting the binding of virus to cell-surface receptors may contribute to the development of antiviral vaccines and therapeutics. Moreover, elucidation of conformational changes induced by the binding of antibodies to viral particles provides an appreciation for the flexibility of viral capsids and contributes to a better understanding of the dynamic nature of nonenveloped viruses.

ACKNOWLEDGMENTS

We thank Jim Chappell and Greg Wilson for careful review of the manuscript and Max Nibert for essential discussions. We express our appreciation to Ken Tyler for providing the 4F2 hybridoma and to Steve Harrison for providing the σ3 X-ray coordinates prior to publication. We acknowledge the National Cell Culture Center for purification of MAbs.

This work was supported by Public Health Service award AI32539 from the National Institute of Allergy and Infectious Diseases and the Elizabeth B. Lamb Center for Pediatric Research.

REFERENCES

1. **Armstrong, G. D., R. W. Paul, and P. W. Lee.** 1984. Studies on reovirus receptors of L cells: virus binding characteristics and comparison with reovirus receptors of erythrocytes. Virology **138:**37–48.
2. **Baer, G. S., and T. S. Dermody.** 1997. Mutations in reovirus outer-capsid protein σ3 selected during persistent infections of L cells confer resistance to protease inhibitor E64. J. Virol. **71:**4921–4928.
3. **Banerjea, A. C., K. A. Brechling, C. A. Ray, H. Erikson, D. J. Pickup, and W. K. Joklik.** 1988. High-level synthesis of biologically active reovirus protein sigma 1 in a mammalian expression vector system. Virology **167:**601–612.
4. **Barton, E. S., J. C. Forrest, J. L. Connolly, J. D. Chappell, Y. Liu, F. J. Schnell, A. Nusrat, C. A. Parkos, and T. S. Dermody.** 2001. Junction adhesion molecule is a receptor for reovirus. Cell **104:**441–451.
5. **Borsa, J., B. D. Morash, M. D. Sargent, T. P. Copps, P. A. Lievaart, and J. G. Szekely.** 1979. Two modes of entry of reovirus particles into L cells. J. Gen. Virol. **45:**161–170.
6. **Burstin, S. J., D. R. Spriggs, and B. N. Fields.** 1982. Evidence for functional domains on the reovirus type 3 hemagglutinin. Virology **117:**146–155.
7. **Carson, M.** 1997. "Ribbons" Methods Enzymol. **277:**493–505.
8. **Centonze, V. E., Y. Chen, T. F. Severson, G. G. Borisy, and M. L. Nibert.** 1995. Visualization of single reovirus particles by low-temperature, high-resolution scanning electron microscopy. J. Struct. Biol. **115:**215–225.
9. **Chappell, J. D., J. Duong, B. W. Wright, and T. S. Dermody.** 2000. Identification of carbohydrate-binding domains in the attachment proteins of type 1 and type 3 reoviruses. J. Virol. **74:**8472–8479.
10. **Chappell, J. D., V. L. Gunn, J. D. Wetzel, G. S. Baer, and T. S. Dermody.** 1997. Mutations in type 3 reovirus that determine binding to sialic acid are contained in the fibrous tail domain of viral attachment protein σ1. J. Virol. **71:**1834–1841.
11. **Crowther, R. A.** 1971. Procedures for three-dimensional reconstruction of

spherical viruses by Fourier synthesis from electron micrographs. Philos. Trans. R. Soc. Lond. **261:**221–230.
12. **Davies, D. R. and H. Metzger.** 1983. Structural basis of antibody function. Annu. Rev. Immunol. **1:**87–117.
13. **Dermody, T. S., M. L. Nibert, R. Bassel-Duby, and B. N. Fields.** 1990. A σ1 region important for hemagglutination by serotype 3 reovirus strains. J. Virol. **64:**5173–5176.
14. **Dryden, K. A., G. Wang, M. Yeager, M. L. Nibert, K. M. Coombs, D. B. Furlong, B. N. Fields, and T. S. Baker.** 1993. Early steps in reovirus infection are associated with dramatic changes in supramolecular structure and protein conformation: analysis of virions and subviral particles by cryoelectron microscopy and image reconstruction. J. Cell Biol. **122:**1023–1041.
15. **Dubochet, J., M. Adrian, J. J. Chang, J. C. Homo, J. Lepault, A. W. McDowall, and P. Schultz.** 1988. Cryo-electron microscopy of vitrified specimens. Q. Rev. Biophys. **21:**129–228.
16. **Ebert, D. H., J. D. Wetzel, D. E. Brumbaugh, S. R. Chance, L. E. Stobie, G. S. Baer, and T. S. Dermody.** 2001. Adaptation of reovirus to growth in the presence of protease inhibitor E64 segregates with a mutation in the carboxy terminus of viral outer-capsid protein σ3. J. Virol. **75:**3197–3206.
17. **Fraser, R. D., D. B. Furlong, B. L. Trus, M. L. Nibert, B. N. Fields, and A. C. Steven.** 1990. Molecular structure of the cell-attachment protein of reovirus: correlation of computer-processed electron micrographs with sequence-based predictions. J. Virol. **64:**2990–3000.
18. **Fuller, S. D.** 1987. The T=4 envelope of Sindbis virus is organized by interactions with a complementary T=3 capsid. Cell **48:**923–934.
19. **Furlong, D. B., M. L. Nibert, and B. N. Fields.** 1988. Sigma 1 protein of mammalian reoviruses extends from the surfaces of viral particles. J. Virol. **62:**246–256.
20. **Gentsch, J. R., and A. F. Pacitti.** 1987. Differential interaction of reovirus type 3 with sialylated receptor components on animal cells. Virology **161:** 245–248.
21. **Gentsch, J. R., and A. F. Pacitti.** 1985. Effect of neuraminidase treatment of cells and effect of soluble glycoproteins on type 3 reovirus attachment to murine L cells. J. Virol. **56:**356–364.
22. **Hooper, J. W., and B. N. Fields.** 1996. Monoclonal antibodies to reovirus σ1 and μ1 proteins inhibit chromium release from mouse L cells. J. Virol. **70:**672–677.
23. **Hooper, J. W., and B. N. Fields.** 1996. Role of the μ1 protein in reovirus stability and capacity to cause chromium release from host cells. J. Virol. **70:**459–467.
24. **Jeffrey, P. D., J. Bajorath, C. Y. Chang, D. Yelton, I. Hellstrom, K. E. Hellstrom, and S. Sheriff.** 1995. The x-ray structure of an anti-tumour antibody in complex with antigen. Nat. Struct. Biol. **2:**466–471.
25. **Jones, T. A., J.-Y. Zou, S. W. Cowan, and M. Kjeldgaard.** 1991. Improved methods for binding protein models in electron density maps and the location of errors in these models. Acta Crystallographa **47:**110–119.
26. **Kedl, R., S. Schmechel, and L. Schiff.** 1995. Comparative sequence analysis of the reovirus S4 genes from 13 serotype 1 and serotype 3 field isolates. J. Virol. **69:**552–559.
27. **Lawton, J. A., and B. V. V. Prasad.** 1996. Automated software package for icosahedral virus reconstruction. J. Struct. Biol. **116:**209–215.
28. **Liu, Y., A. Nusrat, F. J. Schnell, T. A. Reaves, S. Walsh, M. Ponchet, and C. A. Parkos.** 2000. Human junction adhesion molecule regulates tight junction resealing in epithelia. J. Cell Sci. **113:**1–11.
29. **Lucia-Jandris, P., J. W. Hooper, and B. N. Fields.** 1993. Reovirus M2 gene is associated with chromium release from mouse L cells. J. Virol. **67:**5339–5345.
30. **Martin-Padura, I., S. Lostaglio, M. Schneemann, L. Williams, M. Romano, P. Fruscella, C. Panzeri, A. Stoppacciaro, L. Ruco, A. Villa, D. Simmons, and E. Dejana.** 1998. Junctional adhesion molecule, a novel member of the immunoglobulin superfamily that distributes at intercellular junctions and modulates monocyte transmigration. J. Cell Biol. **142:**117–127.
31. **Masri, S. A., L. Nagata, D. C. Mah, and P. W. Lee.** 1986. Functional expression in Escherichia coli of cloned reovirus S1 gene encoding the viral cell attachment protein σ1. Virology **149:**83–90.
32. **Nibert, M. L., J. D. Chappell, and T. S. Dermody.** 1995. Infectious subvirion particles of reovirus type 3 Dearing exhibit a loss in infectivity and contain a cleaved σ1 protein. J. Virol. **69:**5057–5067.
32a. **Olland, A. M., J. Jané-Valbuena, L. A. Schiff, M. L. Nibert, and S. C. Harrison.** 2001. Structure of the reovirus outer capsid and dsRNA-binding protein σ3 at 1.8 Å resolution. EMBO **20:**979–989.
33. **Paul, R. W., A. H. Choi, and P. W. K. Lee.** 1989. The α-anomeric form of sialic acid is the minimal receptor determinant recognized by reovirus. Virology **172:**382–385.
34. **Paul, R. W., and P. W. K. Lee.** 1987. Glycophorin is the reovirus receptor on human erythrocytes. Virology **159:**94–101.
35. **Rubin, D. H., J. D. Wetzel, W. V. Williams, J. A. Cohen, C. Dworkin, and T. S. Dermody.** 1992. Binding of type 3 reovirus by a domain of the σ1 protein important for hemagglutination leads to infection of murine erythroleukemia cells. J. Clin. Investig. **90:**2536–2542.
36. **Spriggs, D. R., and B. N. Fields.** 1982. Attenuated reovirus type 3 strains generated by selection of haemagglutinin antigenic variants. Nature **297:**68–70.
37. **Sturzenbecker, L. J., M. Nibert, D. Furlong, and B. N. Fields.** 1987. Intracellular digestion of reovirus particles requires a low pH and is an essential step in the viral infectious cycle. J. Virol. **61:**2351–2361.
38. **Tyler, K. L., M. A. Mann, B. N. Fields, and H. W. Virgin IV.** 1993. Protective anti-reovirus antibodies and their effects on viral pathogenesis. J. Virol. **67:**3446–3453.
39. **van Heel, M.** 1987. Similarity measures between images. Ultramicroscopy **21:**456–469.
40. **Virgin, H. W., IV, M. A. Mann, B. N. Fields, and K. L. Tyler.** 1991. Monoclonal antibodies to reovirus reveal structure/function relationships between capsid proteins and genetics of susceptibility to antibody action. J. Virol. **65:**6772–6781.
41. **Virgin, H. W., M. A. Mann, and K. L. Tyler.** 1994. Protective antibodies inhibit reovirus internalization and uncoating by intracellular proteases. J. Virol. **68:**6719–6729.
42. **Weiner, H. L., R. F. Ramig, T. A. Mustoe, and B. N. Fields.** 1978. Identification of the gene coding for the hemagglutinin of reovirus. Virology **86:** 581–584.
43. **Wetzel, J. D., G. J. Wilson, G. S. Baer, L. R. Dunnigan, J. P. Wright, D. S. H. Tang, and T. S. Dermody.** 1997. Reovirus variants selected during persistent infections of L cells contain mutations in the viral S1 and S4 genes and are altered in viral disassembly. J. Virol. **71:**1362–1369.
44. **Whitton, J. L., and M. B. A. Oldstone.** 1996. Immune responses to viruses, p. 345–374. *In* B. N. Fields, D. M. Knipe, and P. M. Howley (ed.), Fields virology, 3rd ed. Lippincott-Raven, Philadelphia, Pa.
45. **Wriggers, W., R. A. Milligan, and J. A. McCammon.** 1999. Situs: a package for docking crystal structures into low-resolution maps from electron microscopy. J. Struct. Biol. **125:**185–195.
46. **Zhou, Z. H., B. V. V. Prasad, J. Jakana, F. J. Rixon, and W. Chiu.** 1994. Protein subunit structures in the herpes simplex virus capsid determined from 400-kV spot-scan electron cryomicroscopy. J. Mol. Biol. **242:**456–469.